0090-9556/04/3209-1023–1031$20.00
DRUG METABOLISM AND DISPOSITION
DMD 32:1023–1031, 2004

Vol. 32, No. 9
59/1172935
Printed in U.S.A.

IN VITRO METABOLISM OF MK-0767 [(±)-5-[(2,4-DIOXOTHIAZOLIDIN-5-YL)METHYL]-2-METHOXY-*N*-[[(4-TRIFLUOROMETHYL)-PHENYL] METHYL]BENZAMIDE], A PEROXISOME PROLIFERATOR-ACTIVATED RECEPTOR α/γ AGONIST. II. IDENTIFICATION OF METABOLITES BY LIQUID CHROMATOGRAPHY-TANDEM MASS SPECTROMETRY

David Q. Liu, Bindhu V. Karanam, George A. Doss, Rick R. Sidler, Stella H. Vincent, and Cornelis E.C.A. Hop

Departments of Drug Metabolism (D.Q.L., B.V.K., G.A.D., S.H.V., C.E.C.A.H.) and Process Research (R.R.S.), Merck Research Laboratories, Rahway, New Jersey

Received April 1, 2004; accepted June 22, 2004

ABSTRACT:

The in vitro metabolism of MK-0767 [(±)-5-[(2,4-dioxothiazolidin-5-yl) methyl]-2-methoxy-*N*-[[(4-trifluoromethyl)-phenyl] methyl]benzamide], a novel 2,4-thiazolidinedione (TZD)-containing peroxisome proliferator-activated receptor α/γ agonist, was studied in rat, dog, monkey, and human liver microsomes and hepatocytes, as well as in recombinant human CYP3A4-containing microsomes. Twenty-two metabolites (some at trace levels) were detected by liquid chromatography-tandem mass spectrometry analysis. All appeared to be phase I metabolites except for a glucuronide conjugate of a hydroxylated metabolite that was detected at trace levels. A constant neutral loss scan experiment performed on a triple quadrupole mass spectrometer proved to be very useful for resolving the metabolites from endogenous compounds. It was observed that the initial site of metabolism of MK-0767 was at the TZD ring leading to two major metabolites, namely the 5-hydroxy-TZD metabolite (M24) and the mercapto metabolite (M22). The latter was formed via the cleavage of the TZD ring with the elimination of the carbonyl adjacent to the sulfur atom. The structure of M24 was established by accurate mass measurements and NMR analysis. This hydroxy-TZD metabolite might represent an important precursor for a group of metabolites formed by TZD ring opening and subsequent loss of the sulfur moiety. The mercapto metabolite, on the other hand, is probably the key precursor for the TZD ring-opened metabolites with retention of the sulfur, even though the detailed mechanism of the ring scission remains to be characterized. From these studies, it was concluded that the TZD ring was the major site of metabolism of MK-0767. All the metabolites produced in vitro from human preparations were detected in the corresponding preparations from the nonclinical species.

The thiazolidinedione (TZD)-containing drugs, rosiglitazone and pioglitazone, represent a new class of oral antidiabetic agents for the treatment of type 2 diabetes. These compounds bind to the nuclear peroxisome proliferator-activated receptors (PPARs) in tissues, resulting in the increased expression of genes encoding proteins that are involved in glucose and lipid metabolism (Mudaliar and Henry, 2001). There are three PPAR subtypes, α, γ, and δ. PPARα is highly expressed in hepatocytes, cardiomyocytes, enterocytes, and the proximal tubule cells of kidney, whereas PPARγ is expressed predominantly in adipose tissue and the immune system (Vanden Heuvel, 1999). PPARδ, which is expressed ubiquitously in many tissues, has not been linked to any important clinical manifestation (Kersten et al., 2000).

MK-0767 [(±)-(5-[(2,4-dioxothiazolidin-5-yl)methyl]-2-methoxy-*N*-[[(4-trifluoromethyl)-phenyl] methyl]benzamide; Fig. 1), also known as KRP-297, is a novel 2,4-TZD-containing PPAR agonist (Nomura et al., 1999) that binds to, and activates, both PPARα and PPARγ isoforms with similar affinity (Murakami et al., 1998), whereas pioglitazone and rosiglitazone have been reported to bind to, and activate, primarily the PPARγ receptor.

The objective of this study was to elucidate the in vitro biotransformation pathways of MK-0767 in humans and nonclinical species including rats, dogs, and monkeys. Detection and identification of the metabolites were achieved using liquid chromatography-tandem mass spectrometry with off-line or on-line radiometric monitoring.

Materials and Methods

Chemicals and Reagents. MK-0767 and the synthetic standards of its major metabolites, the methyl sulfoxide carboxylic acid (**M5** and **M9**), the benzoic acid (**M11**), the phenylacetic acid (**M13**), the methyl sulfoxide amide (**M16**), the methyl sulfone amide (**M20**), and the mercapto (**M22**) and the *O*-desmethyl (**M28**) derivatives (Fig. 2) were synthesized at Kyorin Pharmaceutical Co., Ltd. (Tokyo, Japan). [^{14}C]MK-0767 was synthesized by the Labeled Compound Synthesis Group at Merck Research Laboratories in Rah-

Article, publication date, and citation information can be found at http://dmd.aspetjournals.org.
doi:10.1124/dmd.104.000059.

ABBREVIATIONS: TZD, thiazolidinedione; PPAR, peroxisome proliferator-activated receptor; MK-0767, (±)-5-[(2,4-dioxothiazolidin-5-yl)methyl]-2-methoxy-*N*-[[(4-trifluoromethyl)-phenyl] methyl]benzamide; LC-MS, liquid chromatography-mass spectrometry; MS/MS, tandem mass spectrometry; Q-ToF, quadrupole time-of-flight; CID, collision-induced dissociation; HPLC, high-performance liquid chromatography; SAM, *S*-adenosyl methionine.

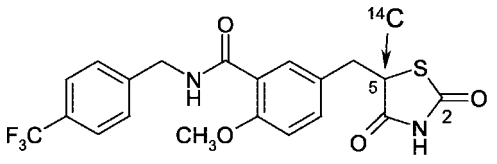

MK-0767

FIG. 1. Chemical structure of [^{14}C]MK-0767.

way, NJ, with a specific activity of ~120 μCi/mg; the position of the ^{14}C atom is indicated in Fig. 1. Methanol (HPLC grade) was purchased from Fisher Scientific Co. (Pittsburgh, PA), and acetonitrile and water (HPLC grade) from Aldrich Chemical Co. (Milwaukee, WI). Glucose 6-phosphate, NADP, glucose-6-phosphate dehydrogenase, *S*-adenosyl methionine (SAM), and ammonium acetate were purchased from Sigma-Aldrich (St. Louis, MO).

Chromatographic and Mass Spectrometric Methods. LC-MS analysis was conducted on a PE Sciex API 3000 mass spectrometer (PerkinElmerSciex Instruments, Boston, MA), which was interfaced with a PerkinElmer HPLC system (PerkinElmer Life and Analytical Sciences, Boston MA) equipped with two Series 200 micro pumps and a PerkinElmer Series 200 autosampler. LC-MS and LC-MS/MS experiments were carried out using the Turbo-Ionspray interface operated in the positive ion mode, except for M7, which was only detectable in the negative ion mode. Full scan MS, product ion scan, and neutral loss scan (loss of 175) experiments were performed on all samples. The temperature of the Turbo-Ionspray auxiliary gas was 350°C and the ionization voltage was 4500 V. The orifice and ring voltages were optimized using MK-0767 and were set to 48 V and 240 V, respectively. High-purity nitrogen (99.9%) was used as the nebulizer, auxiliary, and curtain and collision gas. MS/MS experiments were performed using a collision energy of 42 eV (laboratory frame) and a collision gas thickness of 4. A Zorbax XDB-C8 column (3.0 × 150 mm, 3.5 μm; Mac-Mod Analytical, Chadds Ford, PA) was used for chromatographic separation, and was eluted at 0.5 ml/min with a gradient of 10 mM ammonium acetate in water (A) and 7 mM ammonium acetate in acetonitrile with 7% methanol (B). The gradient was started at 26% B, and increased linearly to 30% B in 5 min, followed by a hold at 30% B for 7 min. It was then increased linearly to 55% B in 20 min, followed by a linear ramp to 90% B in 1 min. The column was washed with 90% B for 4.5 min. One fifth of the flow was directed into the mass spectrometer, and the remainder was used for radiometric detection. This was achieved either by collecting 30-s fractions, followed by liquid scintillation counting, or using an on-line PerkinElmer flow scintillation analyzer where the column eluate was mixed with 3 volumes of PerkinElmer Ultima Flo-M scintillation fluid. Structural confirmation of **M5**, **M9**, **M11, M13, M16**, **M20**, **M22**, and **M28** was achieved by comparing their retention times and MS/MS spectra with those of the authentic standards.

Accurate mass measurements were conducted on a Micromass Q-ToF (quadrupole time-of-flight) II mass spectrometer (Waters, Milford, MA) operated in the positive electrospray ionization mode with the capillary voltage set to 3000 V. The source and desolvation gas temperatures were set at 80°C and 120°C, respectively. The cone voltage and collision energies were 48 V and 30 V, respectively. The instrument was calibrated using a mixture of polyethylene glycols on the day of sample analysis. A small fraction of the purified **M24** was dissolved in a 50:50 (v/v) mixture of methanol and water and infused to the electrospray interface using a syringe pump at a flow rate of 5 μl/min. A residual polyethylene glycol signal was used as the internal lock for measuring the protonated molecule of **M24**. For measurements of the fragment ions, the residual parent ion at *m/z* 455.0889 was used as the reference. Ultrahigh-purity helium was used as the collision gas.

Microsomal Incubations with [^{14}C]MK-0767. [^{14}C]MK-0767 (5 μM) was incubated with rat, dog, monkey, and human liver microsomes pooled from several subjects at a protein concentration of 1 mg/ml in 0.1 M phosphate

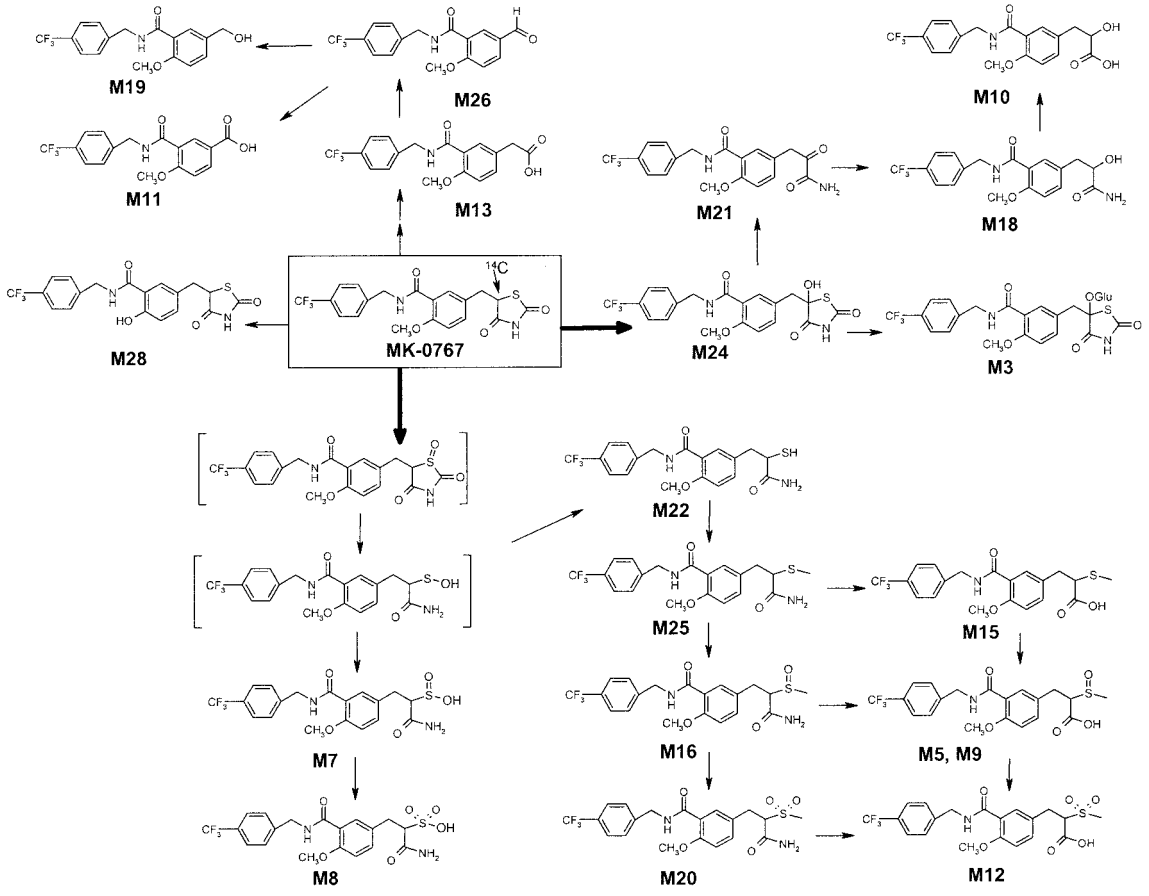

FIG. 2. Proposed biotransformation pathways for MK-0767. Structures in brackets represent likely but unproven intermediates.

buffer containing 1 mM EDTA and 5 mM $MgCl_2$. The reactions were carried out for 30 to 60 min at 37°C in a shaking water bath. Incubations were initiated with the addition of an NADPH-regenerating system, consisting of 10 mM glucose 6-phosphate, 10 mM NADP, and 1.4 units/ml of glucose-6-phosphate dehydrogenase. To generate methylated metabolites of MK-0767, microsomal incubations were fortified with 100 μM SAM before the addition of the NADPH-regenerating system. Control incubations without the NADPH-regenerating system and with SAM alone were carried out under otherwise similar conditions. All incubations were terminated with acetonitrile. After centrifugation at 3000 rpm for 10 min at 4°C, the supernatants were decanted and evaporated under a nitrogen stream. The dried extracts were reconstituted in acetonitrile/water (50:50 v/v) for LC-MS analysis.

Hepatocyte Incubations with [^{14}C]MK-0767. Rat, dog, monkey, and human hepatocytes (1 million cells/ml) were incubated with 5 μM [^{14}C]MK-0767 for 60 min at 37°C and were quenched with acetonitrile in the same way as microsomal samples before LC-MS analysis.

Isolation of Metabolite M24. Metabolite **M24** was isolated from recombinant human CYP3A4 bioreactor incubation (Rushmore et al., 2000) using solid phase extraction followed by HPLC purification. Briefly, the bioreactor incubation mixture was treated with methanol and loaded onto C18 cartridges which were pre-equilibrated with water and methanol. The **M24**-containing fraction was eluted with methanol. The solid phase eluate was injected onto a Zorbax C8 column (4.6 × 250 mm) and eluted from the column with a 30-min gradient from 60% A (10 mM ammonium acetate in water) to 90% B (7 mM ammonium acetate in acetonitrile with 7% methanol). Fractions corresponding to the peak for metabolite **M24** were collected according to UV absorbance at 220 nm. The pooled fractions were evaporated to dryness under nitrogen and the residue was reconstituted in acetonitrile/water (50:50 v/v). The sample was rechromatographed on a pristine column as above, and the pooled fractions were concentrated under nitrogen and subjected to proton NMR and Q-ToF analysis. The structure of **M24** was elucidated based on proton NMR and Q-ToF mass spectrometric data.

NMR Spectroscopy. Proton NMR spectra were acquired on a Varian Inova 600 MHz spectrometer (Varian, Inc., Palo Alto, CA) using a 3-mm probe. Samples were dissolved in dimethyl sulfoxide-d_6. The chemical shifts are expressed in ppm downfield from tetramethylsilane.

Results

Metabolism of MK-0767 in Incubations with Rat, Dog, Monkey, and Human Liver Microsomes, Hepatocytes, and Recombinant Human CYP3A4. The metabolism of [^{14}C]MK-0767 (5 μM) was studied in rat, dog, monkey, and human liver microsomes in the presence of NADPH alone or in combination with SAM, as well as with recombinant human CYP3A4 in the presence of NADPH. In the absence of SAM, the main metabolites in liver microsomal incubations from all species were the 5-hydroxy-TZD (**M24**), mercapto (**M22**), α-hydroxy amide (**M18**), and sulfonic acid (**M8**) metabolites (Fig. 2; Table 1). No metabolism was observed in the absence of NADPH (data not shown). Also, the formation of all metabolites (except **M24**) could be inhibited by a CYP3A4 monoclonal antibody (Karanam et al., 2004). Moreover, incubation with recombinant human CYP3A4 (Fig. 4) generated all of the metabolites detected in liver microsomes from humans and the nonclinical species in the presence of NADPH, except for **M28** (Table 1), indicating that

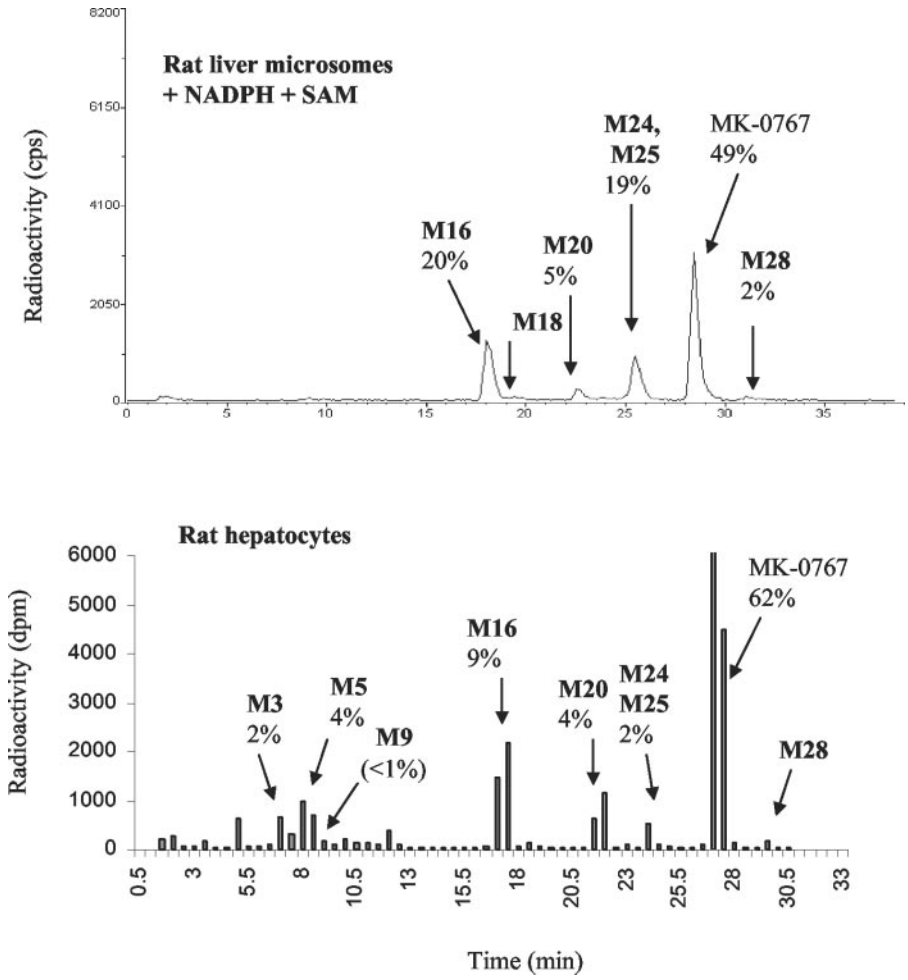

FIG. 3. Representative HPLC-radioactivity profiles of incubations of [^{14}C]MK-0767 in rat SAM- and NADPH-fortified rat liver microsomes and hepatocytes. The percentage values in the chromatograms represent the contribution of each radioactive component in the sample being analyzed.

TABLE 1

Results of LC-MS/MS analysis of in vitro incubations of [^{14}C]MK-0767

Metabolite	*m/z*[a]	Fragment Ions, *m/z*	Retention Time	Occurrence[b]								
				RLM	DLM	MLM	HLM	3A4	RH	DH	MH	HH
			min									
MK-0767	439	322, 264 (B),[c] 193, 159, 148, 120	28.2	+	+	+	+	+	+	+	+	+
M3	631	455 (B), 437, 395, 280, 220	7.2						+		+	
M5[d]	444	336, 207, 205 (B), 192, 187, 166, 161, 159, 134	8.7						+	+	+	
M7	443[e]	379	8.7	+	+	+	+	+				
M8	461	381, 364, 322, 310, 206, 189 (B), 135, 72	9.5	+	+	+	+	+		+		
M9[d]	444	336, 207, 205 (B), 192, 187, 166, 161, 159	9.8						+	+	+	
M10[f]	398	223 (B), 177	10.9	+				+	+		+	
M11[f]	354	179 (B), 159, 121	9.4	+	+	+	+	+	+	+	+	+
M12[d,f]	460	322, 285, 241 (B), 161, 159	11.7						+			+
M13[f]	368	322, 193 (B), 159, 135	12.9	+	+	+	+	+	+		+	+
M15[d,f]	428	322, 253, 207 (B),159, 14	17.1								+	
M16[d]	443	379, 362, 336, 268, 204 (B), 188, 161, 159	18.5	+	+	+	+		+	+	+	+
M18	397	352, 222, 177 (B), 159, 149	19.5	+	+	+	+	+	+		+	+
M19[f]	340	165 (B), 159, 107	21.9	+	+	+	+	+	+			+
M20[d]	459	442, 336, 322, 284 (B), 267, 204, 188, 161, 159, 149	22.9	+	+	+	+		+	+	+	+
M21[f]	395	322, 220, 175 (B), 159, 149	23.8	+	+	+	+	+			+	
M22[f]	413	238, 193 (B), 161	24.6	+	+	+	+	+				
M23[f]	421	350, 246, 175 (B), 159	25.1	+	+	+	+	+	+		+	+
M24	455	395, 322, 280, 220, 175 (B), 159	25.3	+	+	+	+	+	+	+	+	+
M25[d]	427	252, 235, 207 (B)	25.4		+	+	+		+		+	+
M26[f]	338	163 (B), 159, 105	27.3	+	+	+	+	+	+	+	+	+
M27[f]	437	262, 191 (B)	27.8	+	+	+	+	+	+	+	+	+
M28	425	308, 250 (B), 190, 179, 159, 134, 106	30.6	+	+	+	+		+			

[a] All $[M + H]^+$, except as noted.
[b] RLM, DLM, MLM, and HLM denote rat, dog, monkey, and human liver microsomes, respectively; 3A4, recombinant human CYP3A4; and RH, DH, MH, and HH represent rat, dog, monkey, and human hepatocyte suspensions, respectively.
[c] B, base peak; +, detected by mass spectral analysis.
[d] Metabolites formed in the presence of SAM and NADPH; all other metabolites were formed in the presence of NADPH.
[e] $[M - H]^-$.
[f] Minor metabolites.

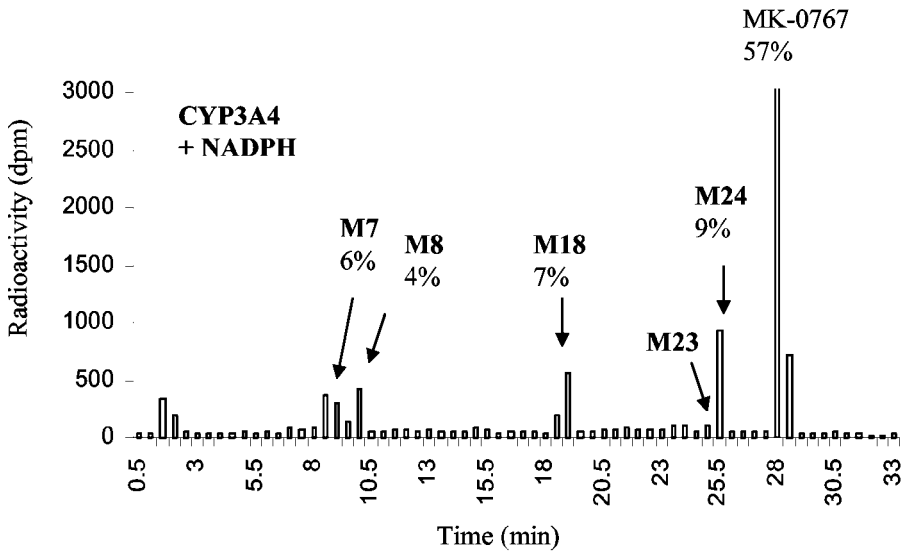

FIG. 4. Representative HPLC-radioactivity profiles of incubations of [^{14}C]MK-0767 with recombinant human CYP3A4 microsomes. The percentage values in the chromatograms represent the contribution of each radioactive component in the sample being analyzed.

CYP3A4 was the major enzyme responsible for the metabolism of MK-0767. The formation of **M28** was catalyzed by CYP2C9 and CYP2C19 (Karanam et al., 2004). Overall, the extent of metabolism in NADPH-fortified liver microsomes was low. As described in the accompanying article (Karanam et al., 2004), addition of the methyl donor, SAM, increased the rate of metabolism and induced the formation of the methyl mercapto (**M25**), methyl sulfoxide amide (**M16**), and methyl sulfone amide (**M20**) metabolites, generating profiles more like those obtained from hepatocyte incubations (Fig. 3). In the presence of SAM, the rat liver microsomes generated the highest turnover followed by human and monkey, and the dog the lowest. Similarly, the extent of metabolism in hepatocytes was highest in rats and lowest in dogs, whereas the extent of metabolism was similar for dog and human hepatocytes. All metabolites produced in human liver microsomes and hepatocytes were detectable in the corresponding preparations from nonclinical species (Table 1).

MS/MS Fragmentation of MK-0767. The collision-induced dissociation (CID) spectrum and major fragment ions of MK-0767 are

shown in Fig. 5. The most intense fragment ion, at *m/z* 264, was formed via a neutral loss of 175 Da, corresponding to the trifluoromethylbenzyl amine moiety. Two additional fragment ions at *m/z* 204 and *m/z* 193 were formed, presumably, via the loss of the neutral species SCO and HNCO + CO, respectively, from *m/z* 264. A fragment ion at *m/z* 322, formed by the loss of the TZD ring, was useful in elucidating the location of the biotransformation. For example, the presence of the *m/z* 322 fragment in a metabolite indicated that the biotransformation had occurred on the TZD ring.

Identification of M3. Metabolite **M3** gave a protonated molecule $[M + H]^+$ at *m/z* 631. Loss of 176 Da gave a fragment with *m/z* 455 corresponding to an oxygenated form of MK-0767. Neutral loss of 175 Da from *m/z* 455 afforded the fragment at *m/z* 280, indicating that the oxidation had occurred on the TZD ring. Thus, **M3** was proposed as a glucuronide conjugate of metabolite **M24** (see below for identification of **M24**).

Identification of M5, M9, and M12. Two radioactive peaks, eluting at 8.7 and 9.8 min (**M5** and **M9**), respectively, gave rise to protonated molecules $[M + H]^+$ at *m/z* 444 and produced identical CID spectra. The *m/z* 269 ion, resulting from neutral loss of 175 Da, was not observed because it fragmented by loss of the methyl sulfoxide moiety to give an *m/z* 205 ion. Elimination of the methyl sulfoxide moiety and CO_2 from the protonated molecule gave rise to *m/z* 336; subsequent neutral loss of 175 Da from *m/z* 336 produced *m/z* 161. Collectively, this fragmentation pattern suggested that **M5** and **M9** were the methyl sulfoxide carboxylic acid derivatives. The structures were confirmed by comparison with authentic standards. Metabolite **M12** was a minor component. It produced a protonated molecule $[M + H]^+$ at *m/z* 460, 16 units higher than that of **M5** or **M9**. This suggested that it could be an oxygenated derivative of **M5** or **M9**. Neutral loss of 175 Da gave *m/z* 285. Further loss of CO_2 afforded the most intense ion at *m/z* 241. A minor signal at *m/z* 322 suggested that the biotransformation had occurred on the TZD ring. Therefore, the methyl sulfonyl carboxylic acid structure was proposed for metabolite **M12** (Fig. 2).

Identification of M7 and M8. Metabolite **M7** was detectable only in the negative ionization mode. The deprotonated molecule $[M - H]^-$ was observed at *m/z* 443. The fragment ion at *m/z* 379 was formed via elimination of SO_2. Therefore, **M7** was proposed as the sulfinic acid metabolite, which was presumably the precursor of metabolite **M8**, a sulfonic acid. Metabolite **M8** gave a protonated molecule $[M + H]^+$ at *m/z* 461 in the positive ion mode and a deprotonated molecule, $[M - H]^-$, at *m/z* 459 in the negative ion mode. In the positive ion mode, a trace amount of *m/z* 381, corresponding to loss of SO_3, was observed. Further loss of NH_3 from *m/z* 381 gave *m/z* 364. Neutral loss of 175 Da from *m/z* 364 afforded a fragment at *m/z* 189 as the base peak. In addition, neutral loss of 175 Da from *m/z* 381 was observed, leading to the *m/z* 206 ion. The sulfonic acid structure was thus proposed for **M8**. The assigned structure was supported by accurate mass measurements conducted on a Q-ToF instrument. Using an internal lock at the parent mass of *m/z* 461, the mass difference between *m/z* 461 and *m/z* 364 was measured to be 96.9836 Da, whereas the calculated mass for $NH_3 + SO_3$ was 96.9834 Da. This represented a difference of 2.4 ppm, the only match with less than 25 ppm of error.

Identification of M10, M18, and M21. A minor metabolite, **M10**, gave a protonated molecule $[M + H]^+$ at *m/z* 398, which produced *m/z* 223 (neutral loss of 175 Da) upon CID. Further fragmentation of *m/z* 223 gave rise to *m/z* 177 via elimination of HCOOH. Therefore, an α-hydroxyl carboxylic acid structure was assigned to **M10**. Metabolite **M18** gave a protonated molecule $[M + H]^+$ at *m/z* 397, 1 unit less than that of **M10**. Two major product ions were observed at *m/z* 222 via neutral loss of 175 Da and *m/z* 177 via elimination of a formamide from *m/z* 222, respectively. Therefore, an α-hydroxyl amide structure was tentatively proposed for **M18.** Metabolite **M21** exhibited a protonated molecule $[M + H]^+$ at *m/z* 395, 2 units lower than metabolite **M18**. Similar to **M18**, two major signals were observed at *m/z* 220 (neutral loss of 175 Da) and *m/z* 175 (elimination of formamide from *m/z* 220), respectively. Both fragments were 2 mass units less than those of **M18**, indicating that it might be a dehydrogenation derivative of **M18**. A signal at *m/z* 322 confirmed that the biotransformation had occurred on the TZD ring. Thus, an α-keto amide structure was proposed for **M21** (Fig. 2). The relative HPLC retention times of these three metabolites were compatible with their polarity.

Identification of M11, M19, and M26. The mass spectral signal of these metabolites was weak. Also, no radioactivity was associated with these metabolites, indicating that they were minor and/or that they had lost the methine carbon of the TZD ring. These metabolites were detected by a neutral loss scan of 175 Da (Fig. 6). Metabolite **M11** exhibited a protonated molecule $[M + H]^+$ at *m/z* 354, which was detected by a constant neutral loss scan in the triple quadrupole

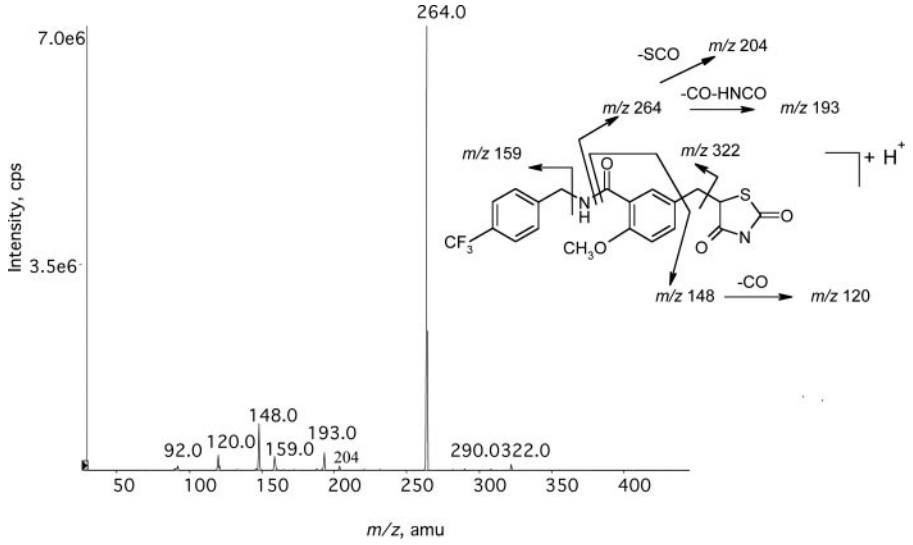

FIG. 5. MS/MS spectrum of MK-0767 and tentative assignments of the fragment ions.

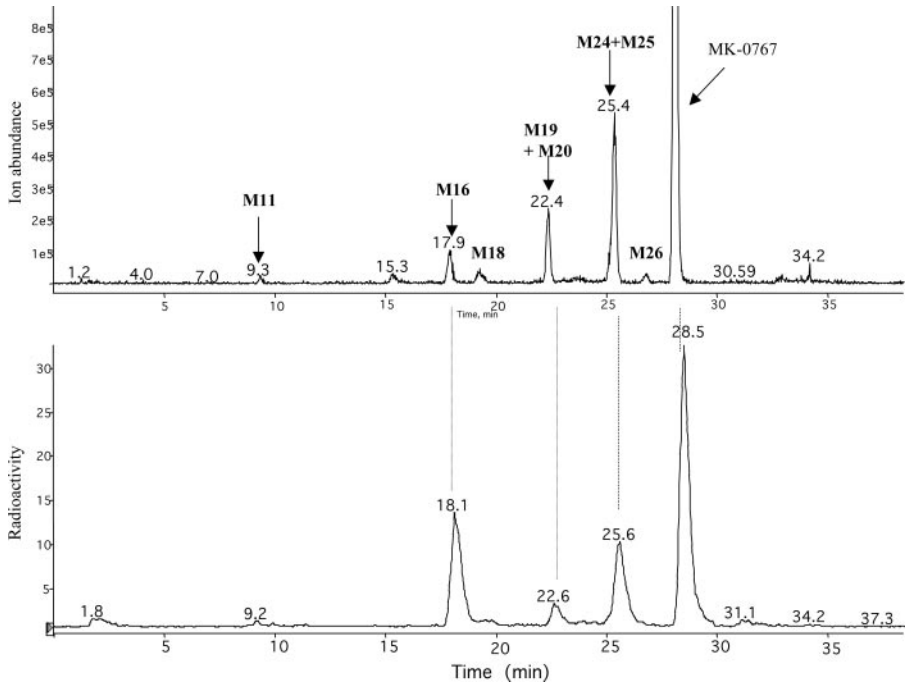

FIG. 6. LC-MS total ion current from a constant neutral loss scan experiment (loss of 175 Da, the trifluoromethylbenzyl amine moiety) (upper trace) and HPLC radiochromatogram of a rat liver microsomal incubation of [^{14}C]MK-0767 (lower trace). The neutral loss scan LC-MS experiment was useful in distinguishing metabolites from the endogenous components.

mass spectrometer. Major fragment ions were observed at *m/z* 179 (neutral loss of 175 Da), *m/z* 159 (corresponding to the trifluoromethylbenzyl moiety), and *m/z* 121 (assigned to the benzoic acid fragment). Thus, a benzoic acid structure was proposed for **M11** (Fig. 2). A synthetic standard was used to confirm its identity. Metabolite **M26** gave a protonated molecule $[M + H]^+$ at *m/z* 338, which was 16 units lower than **M11**. The corresponding fragment at *m/z* 163 was also 16 units lower than that of **M11**. Loss of formaldehyde and a carbonyl group gave rise to the fragment at *m/z* 105. Thus, a benzaldehyde structure was proposed for **M26**, which was, presumably, the precursor of **M11**. Metabolite **M19** had a protonated molecule $[M + H]^+$ at *m/z* 340, 2 units higher than that of metabolite **M26**. The only observed fragment at *m/z* 165 was 2 units higher than the corresponding ion of **M26**. Thus, a benzyl alcohol structure was tentatively assigned to **M19,** which could be formed via reduction of the aldehyde group of **M26**. Again, the relative retention times of these three metabolites were compatible with their polarity.

Identification of M13. Metabolite **M13** gave a protonated molecule $[M + H]^+$ at *m/z* 368. Its MS/MS spectrum showed an intense ion at *m/z* 193 corresponding to the neutral loss of 175 Da. A signal at *m/z* 322 suggested that the portion of the parent molecule, other than the TZD ring, was intact. Therefore, a phenylacetic acid structure was proposed (Fig. 2), which was confirmed by comparison with an authentic standard.

Identification of M15 and M25. The protonated molecule $[M + H]^+$ of **M15** was observed at *m/z* 428. The CID of *m/z* 428 ion afforded two major fragment ions at *m/z* 253 and *m/z* 207. The former resulted from the neutral loss of 175 Da and the latter was formed by the further loss of formic acid. Again, a minor signal at *m/z* 322 indicated that the portion of the parent molecule, other than the TZD ring, was intact. Thus, a methyl mercapto carboxylic acid structure was proposed for **M15** (Fig. 2). The protonated molecule $[M + H]^+$ of **M25** was observed at *m/z* 427, which was 1 unit less than that of **M15**. Similar to **M15**, its MS/MS spectrum exhibited two major fragment ions at *m/z* 252 and *m/z* 207. Elimination of formamide from *m/z* 252 gave *m/z* 207, and loss of NH_3 from *m/z* 252 afforded *m/z* 235. These observations led to the proposal of the methyl mercapto structure for **M25** (Fig. 2).

Identification of M16 and M20. One of the major metabolites, **M16**, gave a protonated molecule $[M + H]^+$ at *m/z* 443, which was 1 unit lower than that of **M5** and **M9**. The mass spectral fragmentation appeared to be analogous to that of **M5** and **M9**. Loss of the methyl sulfinyl and the amide groups gave rise to *m/z* 336. Neutral loss of 175 Da from *m/z* 336 gave *m/z* 161. Thus, the methyl sulfoxide amide structure was proposed and was confirmed by comparison with an authentic standard. Metabolite **M20** gave a protonated molecule $[M + H]^+$ at *m/z* at 459, which was 16 units higher than **M16**, suggesting that it could be a further oxidation product of **M16**. A minor peak, indicating the loss of NH_3, was observed at *m/z* 442. Similar to **M16**, two fragment ions at *m/z* 336 and *m/z* 161 were observed. In addition, an intense signal was observed at *m/z* 322, indicating that the structural portion other than the TZD ring was intact. Taken together, these observations suggested that **M20** had a methyl sulfonyl amide structure, which was confirmed by comparison with an authentic standard. It is noteworthy that the amides **M25**, **M16**, and **M20** eluted consistently approximately 8 to 11 min after their corresponding carboxylic acids, **M15**, **M5** (or **M9**), and **M12**.

Identification of M22. Metabolite **M22** gave a protonated molecule $[M + H]^+$ at *m/z* 413. Neutral loss of 175 Da afforded the fragment ion at *m/z* 238. Further elimination of formamide gave *m/z* 193. Therefore, the mercapto structure was assigned to **M22** (Fig. 2), which was confirmed by comparison with the authentic standard.

Identification of M23 and M27. Metabolite **M23** gave a protonated molecule $[M + H]^+$ at *m/z* 421. Similar to most of the other metabolites, it gave a strong signal for neutral loss of 175 Da at *m/z* 246. In addition, the signal at *m/z* 159, corresponding to the trifluoromethylbenzyl, was observed, indicating that the trifluoromethylbenzyl amine moiety was intact. The only remaining fragment ion was the base peak at *m/z* 175, which could not be assigned. Therefore, the structure of **M23** remains to be established. However, the even mo-

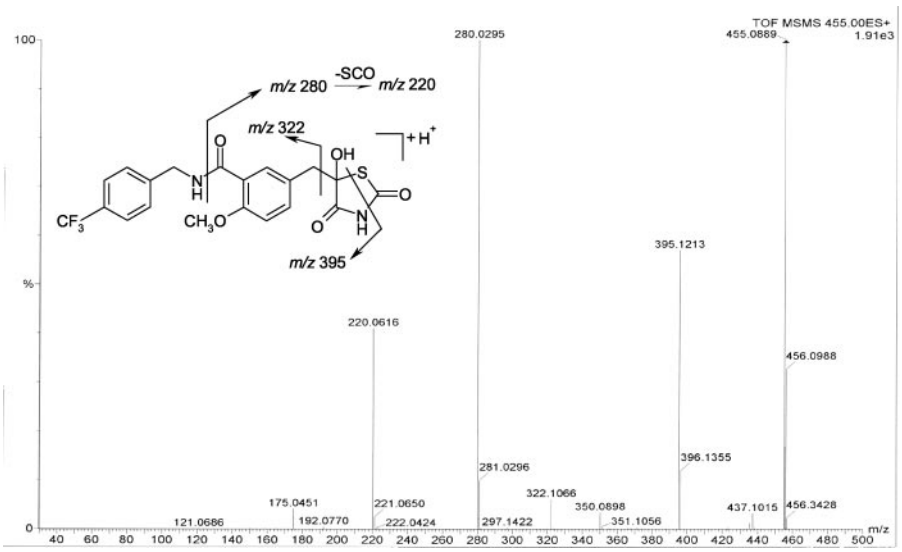

FIG. 7. MS/MS spectrum of metabolite **M24** obtained on a Q-ToF instrument and the assignments of the fragment ions. The accurate mass measurement data are summarized in Table 2.

lecular weight of **M23** indicated that the nitrogen atom of the TZD ring had been retained. **M23,** eluting before the peak containing **M24** and **M25**, was a relatively low abundance metabolite when compared with **M25**. Metabolite **M27** was detected at trace levels and gave a protonated molecule $[M + H]^+$ at *m/z* 437, which was 16 units higher than that of metabolite **M23**. Fragment ions were detected at *m/z* 262 and *m/z* 191 and, both were 16 units higher than the corresponding fragment ions of **M23**. Therefore, **M27** must be an oxygenated derivative of **M23**.

Identification of M24. Metabolite **M24** gave a protonated molecule $[M + H]^+$ at *m/z* 455, which was 16 units higher than that of the parent compound, MK-0767. It appeared to be an oxygenated derivative of the parent. Accurate mass measurements by a Q-ToF instrument revealed the $[M + H]^+$ of **M24** at *m/z* 455.0958, which was within 15.3 ppm of the calculated mass of $[MK\text{-}0767 + O + H]^+$, using a residual polyethylene glycol signal as the internal lock mass. The accuracy of the mass measurement was slightly reduced due to the presence of relatively intense background signals. The MS/MS spectrum of **M24** is presented in Fig. 7. The observed and calculated *m/z* values of the most abundant fragment ions are shown in Table 2. In this experiment the residual parent ion signal was used as the internal lock mass. The most abundant fragment ion had an *m/z* value of 280, which was 16 units higher than the most abundant fragment ion in the spectrum of MK-0767 (Fig. 5). The signal at *m/z* 322 observed in the spectrum of MK-0767 was observed also in the spectrum of **M24**, indicating that the biotransformation had occurred on the TZD ring. The signal at *m/z* 395.1213 was compatible with the loss of SCO from **M24**. Indeed, the measured mass of this fragment ion was within 1.4 ppm of the calculated mass of $[MK\text{-}0767 + O - SCO + H]^+$. In addition, a small signal at *m/z* 437 was visible in the MS/MS spectrum, which could not be observed using a triple quadrupole mass spectrometer. This signal pointed to the loss of H_2O from the protonated molecule of **M24**. The loss of H_2O and SCO suggested that **M24** had the 5-hydroxy-TZD structure shown in Fig. 7 and not the sulfoxide-TZD (Fig. 2), a possible intermediate leading to the TZD ring opening (Kassahun et al., 2001). Hydroxylation of the methine carbon of the TZD ring has been postulated previously (Fouda et al., 1991). It appears that hydroxylation of the methine carbon of the TZD ring facilitated the ring opening fragmentation with simultaneous elimination of SCO. Formation of a stable α-keto amide fragment ion at *m/z* 395 could be the primary driving force for the TZD ring opening. The 5-hydroxy-TZD structure (**M24**) was also confirmed by NMR analysis. The proton NMR spectrum (Fig. 8) showed the loss of H-5 of the TZD ring (the proton on C-5 appeared at 4.86 ppm in the parent compound as dd $J = 4.5, 8.8$ Hz). The benzylic CH_2 protons adjacent to the TZD ring appeared as a simple AB pattern ($J = 13.7$ Hz), which further confirmed the loss of H-5. Other signals were similar to the parent compound. The NMR data are summarized as follows: **MK-0767:** 11.97 (1H, s), 8.77 (1H, t, $J = 6.2$ Hz), 7.65 (2H, d, $J = 8.1$ Hz), 7.59 (1H, d, $J = 2.1$), 7.50 (2H, d, $J = 8.1$ Hz), 7.31 (1H, dd, $J = 8.5, 2.0$ Hz), 7.07 (1H, d, $J = 8.5$ Hz), 4.86 (1H, dd, $J = 4.5, 8.8$ Hz), 4.53 (1H, d, $J = 5.9$ Hz), 3.83 (3H, s), 3.29 (1H, dd, $J = 4.5, 14.1$ Hz), 3.09 (1H, d, $J = 8.8, 14.1$ Hz). **Metabolite M24:** 11.96 (1H, s), 8.74 (1H, t, $J = 5.8$ Hz), 7.65 (2H, d, $J = 8.2$ Hz), 7.61 (1H, d, $J = 1.9$), 7.50 (2H, d, $J = 8.2$ Hz), 7.31 (1H, dd, $J = 8.4, 1.9$ Hz), 7.00 (1H, d, $J = 8.4$ Hz), 4.53 (1H, d, $J = 5.9$ Hz), 3.83 (3H, s), 3.09 (1H, d, $J = 13.7$ Hz), 2.96 (1H, d $J = 13.7$ Hz).

TABLE 2

*Observed and calculated m/z values of the most abundant fragment ions in the MS/MS spectrum of metabolite **M24***

The calculated values and formulas are based on the fragmentation assigned in Fig. 7. The MS/MS spectrum was obtained using a Micromass Q-ToF mass spectrometer (see text for details).

Fragment	Observed *m/z*	Calculated *m/z*	Error	Formula
			ppm	
A	395.1213	395.1219	−1.4	$C_{19}H_{18}N_2O_4F_3$
B	322.1066	322.1055	3.5	$C_{17}H_{15}NO_2F_3$
C	280.0295	280.0280	5.5	$C_{12}H_{10}NO_5S$
D	220.0616	220.0610	2.8	$C_{11}H_{10}NO_4$

Identification of M28. Metabolite **M28** gave a protonated molecule $[M + H]^+$ at *m/z* 425, 14 units lower than that of MK-0767. Neutral loss of 175 Da led to the fragment at *m/z* 250 and the presence of an intense signal at *m/z* 159 suggested that the trifluoromethylbenzyl moiety was unchanged. The fragment ion at *m/z* 308 was 14 units lower than the corresponding fragment ion observed for the parent compound (*m/z* 322), suggesting that the TZD ring was still intact. Thus, the desmethyl structure was proposed for **M28** (Fig. 2), and was confirmed by comparison with an authentic standard.

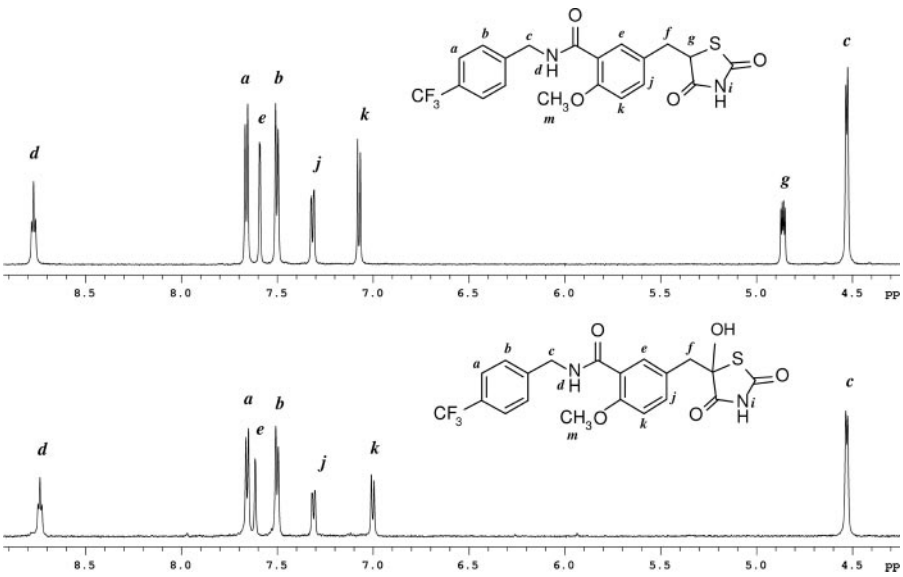

FIG. 8. A detailed region of the ^{1}H NMR spectrum of metabolite **M24** (lower trace) compared with that of the parent compound (upper trace).

Discussion

The present evaluation of the in vitro metabolism of MK-0767 at a pharmacologically relevant concentration (5 μM) in liver microsomes and hepatocytes led to the detection of 22 metabolites, many of which were present at trace levels. A constant neutral loss scan experiment performed on a triple quadrupole mass spectrometer proved to be very useful for differentiating metabolite peaks from endogenous compounds, and for detecting metabolites formed by loss of the ^{14}C label of the TZD ring, e.g., **M11**, **M19**, and **M26** (Fig. 6). Based on the present work, the proposed biotransformation scheme for MK-0767 is illustrated in Fig. 2. Besides the desmethyl metabolite (**M28**) and two unidentified metabolites (**M23** and **M27**), the structures of the identified metabolites indicated that TZD ring opening was the main metabolic route for MK-0767 in vitro. The TZD ring opening of MK-0767 appeared to proceed via two main pathways, i.e., methine *C*-oxidation (hydroxylation) leading to metabolites with loss of sulfur, and *S*-oxidation leading to the sulfur-containing metabolites (see discussion below).

TZD Ring Opening via *C*-Oxidation (Hydroxylation). A major oxidative metabolite, **M24**, was unambiguously identified to have the 5-hydroxy-TZD structure (Fig. 2) by accurate mass measurements using the Micromass Q-ToF II and proton NMR analysis. Metabolite **M24** could be an important precursor leading to the formation of the TZD ring-opened metabolites missing the sulfur moiety. Such a pathway could involve ring opening of **M24** to give the α-keto amide metabolite, **M21**. Reduction of the keto would lead to the formation of the α-hydroxy amide metabolite, **M18**, which could undergo hydrolysis to form the α-hydroxy carboxylic acid, **M10**. Metabolite **M13** could arise from **M10** via decarboxylation; other pathways directly from the parent compound cannot be ruled out. Decarboxylation of **M13** would give metabolite **M26**, a benzyl aldehyde derivative, which can either undergo oxidation leading to the benzoic acid, **M11**, or reduction leading to the benzyl alcohol, **M19.**

TZD Ring Opening via *S*-Oxidation. The mercapto metabolite, **M22**, which was one of the metabolites detected in CYP3A4 incubations (Table 1), most likely served as the key precursor leading to the other TZD ring-opened metabolites with retention of the sulfur. The formation of this thiol structure could be initiated by oxidation at the sulfur to form the sulfoxide, followed by spontaneous hydrolytic cleavage to open the TZD ring and give an intermediate sulfenic acid (Fig. 2). Disproportionation or reduction of the sulfenic acid would give rise to the mercapto metabolite **M22**. This mechanism was proposed for the TZD ring opening of troglitazone by Kassahun et al. (2001). A similar mechanism was also proposed by Hackett et al. (1993) and Nadeau et al. (1993) for the metabolism of the herbicide, triallate. Direct oxidation of **M22** to give **M7**, although possible, was not detected when **M22** was incubated with NADPH-fortified liver microsomes. Therefore, a more likely mechanism for the formation of the sulfinic acid (**M7**) and sulfonic acid (**M8)** is via oxidation of the presumed intermediate sulfenic acid. In the presence of the methyl donor SAM, **M22** underwent methylation to give the methyl mercapto metabolite, **M25**. Sequential *S*-oxidation of **M25** led to the formation of the methyl sulfoxide amide, **M16**, and the methyl sulfone amide, **M20,** as described in detail elsewhere (Karanam et al., 2004). Hydrolysis of **M25**, **M16**, and **M20** (all amides) gave rise to the corresponding carboxylic acid derivatives, **M15**, **M5** (or **M9**), and **M12**, respectively, all presumably mediated by esterases. The detailed mechanism of the TZD ring opening remains to be explored.

The metabolism of the therapeutic glitazones pioglitazone, rosiglitazone, and troglitazone has been examined in detail and, in all cases, very little or no metabolism of the TZD ring itself was detected. Pioglitazone was reported to be modified mainly at the aliphatic ethyl groups (Krieter et al., 1994; Kiyota et al., 1997), whereas rosiglitazone was shown to be metabolized primarily by *para*-hydroxylation and *N*-demethylation (Baldwin et al., 1999; Cox et al., 2000). More recently, Kassahun et al. (2001) and Shen et al. (2003) demonstrated, respectively, that the TZD ring in troglitazone and pioglitazone could undergo oxidative cleavage.

Although TZD ring cleavage has been implicated in the bioactivation of troglitazone (Kassahun et al., 2001), there is no direct evidence linking this mechanism to hepatotoxicity. Moreover, in the case of MK-0767, the TZD ring-opened product, **M22**, was found to undergo facile *S*-methylation and *S*-oxidation. The major metabolites in vivo in all species examined, including humans, were the *S*-methylated **M25**, **M16**, **M20**, **M5**, and **M9**, whereas **M22** itself was present only at trace level. More importantly, MK-0767 was not hepatotoxic in either animals or humans. It should also be noted that TZD cleavage resulted in loss of pharmacological activity, since of all the metabolites tested (**M5**, **M9**, **M11**, **M13**, **M16**, **M20**, **M22**, **M25**, and **M28**), only **M28** retained some PPARγ receptor activity (IC_{50}

~15 μM, compared with ~0.2 μM for MK-0767, and >50 μM for all the other metabolites; unpublished results).

MK-0767 is racemic, containing a 1:1 ratio of *R* and *S* isomers (referring to the methine carbon at the 5 position of the TZD ring), which interconvert rapidly in an aqueous environment. Introduction of a second chiral center via *S*-oxidation would result in a pair of diastereoisomers for each *R* or *S* isomer (total of four diastereoisomers) for the methyl sulfoxide carboxylic acid (**M5** and **M9**) and the methyl sulfoxide amide (**M16**). It appeared that the pairs of diastereoisomers of the acid but not the amide were resolved on the reversed phase C8 column. This was probably due to strong H-bonding between the carboxylic acid hydrogen and the sulfinyl oxygen in the carboxylic acids **M5** and **M9**.

Identification of the enzymes involved in the metabolism of MK-0767 is discussed in the accompanying article (Karanam et al., 2004.). It was demonstrated that ketoconazole almost completely inhibited the in vitro metabolism of MK-0767. The current study showed that the recombinant human CYP3A4 incubation produced almost all the oxidative metabolites detected in NADPH-fortified rat, dog, monkey, or human liver microsomes. Collectively, these data suggested that the metabolism of MK-0767 was mainly CYP3A4-mediated. Esterases and methyltransferases appeared to be involved to a certain extent in the secondary metabolism. The presence of SAM induced the formation of the methylated metabolites. All metabolites produced in human liver microsomes were detected in rat, dog, or monkey microsomes, whereas all those in human hepatocytes were detected in rat, dog, or monkey hepatocytes. From this study, it was concluded that the TZD ring was the dominant site of metabolism of MK-0767. This is the first example of a glitazone that is metabolized predominantly on the TZD ring.

Acknowledgments. We are grateful to Kyorin scientists for the supply of MK-0767 and synthetic standards of its major metabolites; Mike A. Wallace, Dr. Conrad Raab, and Dr. Dennis Dean (Labeled Compound Synthesis Group, Merck Research Laboratories, Rahway, NJ) for the synthesis of [^{14}C]MK-0767; and Dr. Tom Rushmore (Drug Metabolism, Merck Research Laboratories, West Point, PA) for the scale up of the CYP3A4 bioreactor incubation. We would like to acknowledge Dr. Ronald B. Franklin for critical review of the manuscript.

References

Baldwin SJ, Clarke SE, and Chenery RJ (1999) Characterization of the cytochrome P450 enzymes involved in the *in vitro* metabolism of rosiglitazone. *Br J Clin Pharmacol* **48:**424–432.

Cox PJ, Ryan DA, Hollis FJ, Harris AM, Miller AK, Vousden M, and Cowley H (2000) Absorption, distribution and metabolism of rosiglitazone, a potent thiazolidinedione insulin sensitizer, in humans. *Drug Metab Dispos* **28:**772–780.

Fouda HG, Lukaszewicz J, Clark DA, and Hulin B (1991) Metabolism of a new thiazolidinedione hypoglycemic agent CP-68,722 in rats: metabolite identification by gas chromatography mass spectrometry. *Xenobiotica* **21:**925–934.

Hackett AG, Kotyk JJ, Fujiwara H, and Logusch EW (1993) Metabolism of triallate in Sprague-Dawley rats. 3. In vitro metabolic pathways. *J Agric Food Chem* **41:**141–147.

Karanam BV, Hop CECA, Liu DQ, Wallace M, Dean D, Satoh H, Komuro M, Awano K, and Vincent S (2004) In vitro metabolism of MK-0767 (5-[2,4-dioxothiazolidin-5-yl)methyl]-2-methoxy-*N*-[[(4-trifluoromethyl)-phenyl] methyl]benzamide), a peroxisome proliferator-activated receptor PPAR dual agonist. I. Role of cytochrome P450, methyltransferases, flavin monooxygenases, and esterases. Drug Metab Dispos **32:**1015–1022.

Kassahun K, Pearson PG, Tang W, McIntosh I, Leung K, Elmore C, Dean D, Wang R, Doss G, and Baillie TA (2001) Studies on the metabolism of troglitazone to reactive intermediates in vitro and in vivo. Evidence for novel biotransformation pathways involving quinone methide formation and thiazolidinedione ring scission. *Chem Res Toxicol* **14:**62–72.

Kersten S, Desvergne B, and Wahli W (2000) Roles of PPARs in health and disease. *Nature (Lond)* **405:**421–424.

Kiyota Y, Kondo T, Maeshiba Y, Hashimoto A, Yamashita K, Yoshimura Y, Motohashi M, and Tanayama S (1997) Studies on the metabolism of the new antidiabetic agent pioglitazone. Identification of metabolites in rats and dogs. *Arzneim-Forsch/Drug Res* **47:**22–28.

Krieter PA, Colletti AE, Doss GA, and Miller RR (1994) Disposition and metabolism of the hypoglycemic agent pioglitazone in rats. *Drug Metab Dispos* **22:**625–630.

Mudaliar S and Henry RR (2001) New oral therapies for type 2 diabetes mellitus: the glitazones or insulin sensitizers. *Annu Rev Med* **52:**239–257.

Murakami K, Tobe K, Ide T, Mochizuki T, Ohashi M, Akanuma Y, Yazaki Y, and Kadowaki T (1998) A novel insulin sensitizer acts as a coligand for peroxisome proliferator-activated receptor-α (PPAR-α) and PPAR-γ. *Diabetes* **47:**1841–1847.

Nadeau RG, Chott RC, Fujiwara H, Shieh HS, and Logusch EW (1993) Metabolism of triallate in Sprague-Dawley rats. 2. Identification and quantitation of excreted metabolites. *J Agric Food Chem* **41:**132–140.

Nomura M, Kinoshita S, Satoh H, Maeda T, Murakami K, Tsunoda M, Miyachi H, and Awano K (1999) 3-Substituted (benzyl)thiazolidine-2,4-diones as structurally new antihyperglycemic agents. *Bioorg Med Chem Lett* **9:**533–538.

Rushmore TH, Reider PJ, Slaughter D, Assang C, and Shou M (2000) Bioreactor systems in drug metabolism: synthesis of cytochrome P450-generated metabolites. *Metab Eng* **2:**115–125.

Shen Z, Reed JR, Creighton M, Liu DQ, Tang YS, Hora DF, Feeney W, Bakhtiar R, Franklin RB, and Vincent SH (2003) Identification of novel metabolites of pioglitazone in rats and dogs. *Xenobiotica* **33:**499–509.

Vanden Heuvel JP (1999) Peroxisome proliferator-activated receptors (PPARs) and carcinogenesis. *Toxicol Sci* **47:**1–8.

Address correspondence to: Bindhu V. Karanam, Merck Research Laboratories, Department of Drug Metabolism, RY80L-109, P.O. Box 2000, Rahway, NJ 07065. E-mail: bindhu_karanam@merck.com